



# Synthesis and magnetic properties of antiferromagnetic $\text{Co}_3\text{O}_4$ nanoparticles

H.T. Zhu<sup>a,b</sup>, J. Luo<sup>a,\*</sup>, J.K. Liang<sup>a,c</sup>, G.H. Rao<sup>a</sup>, J.B. Li<sup>a</sup>, J.Y. Zhang<sup>a</sup>, Z.M. Du<sup>b</sup>

<sup>a</sup> Beijing National Laboratory for Condensed Matter Physics, Institute of Physics, Chinese Academy of Sciences, Beijing 100190, China

<sup>b</sup> Department of Materials Science and Engineering, University of Science and Technology Beijing, Beijing 100083, China

<sup>c</sup> International Center for Materials Physics, Chinese Academy of Sciences, Shenyang 110016, China

## ARTICLE INFO

### Article history:

Received 5 January 2008

Received in revised form

4 March 2008

Accepted 26 March 2008

### PACS:

75.50.Tt

75.50.Ee

75.75.+a

### Keywords:

Nanoparticles

Antiferromagnetism

Finite size effects

## ABSTRACT

Antiferromagnetic  $\text{Co}_3\text{O}_4$  nanoparticles with diameter around 30 nm have been synthesized by a solution-based method. The phase identification by the wide-angle X-ray powder diffraction indicates that the  $\text{Co}_3\text{O}_4$  nanoparticle has a cubic spinel structure with a lattice constant of 0.80843(2) nm. The image of field emission scanning electron microscope shows that the nanoparticles are assembled together to form nanorods. The magnetic properties of  $\text{Co}_3\text{O}_4$  fine particles have been measured by a superconducting quantum interference device magnetometer. A deviation of the Néel temperature from the bulk is observed, which can be well described by the theory of finite-size scaling. An enhanced coercivity as well as a loop shift are observed in the field-cooled hysteresis loop. The exchange bias field decreases with increasing temperature and diminishes at the Néel temperature. The training effect and the opening of the loop reveal the existence of the spin-glass-like surface spins.

© 2008 Elsevier B.V. All rights reserved.

## 1. Introduction

Magnetism of nanostructured materials has attracted considerable attention by virtue of their unique magnetic properties as well as their prominent application potentials [1–7]. Normally, the antiferromagnetic (AFM) materials have only limited applications due to the complete canceling of the antiparallely aligned magnetic moment. However, increasing interest has been generated for the AFM nanoparticles since the discovery of their potentials for exhibiting magnetization reversal by quantum tunneling [8,9], their uncompensated magnetization below Néel temperature [10–14], and their applications in spin-valve systems, etc. [15]. As for the magnetic properties of AFM nanoparticles, the small size and large surface play a significant role. Néel [16] suggested that fine particles of AFM materials should exhibit superparamagnetism or weak ferromagnetism, which was ascribed to the uncompensated spins on two sublattices. Kodama et al. [11] proposed a multisublattice configuration, indicating a new finite size effect, in which the reduced coordination of the surface spins led to a fundamental change in the magnetic order of the whole particle.

Recently, the research on synthesis and magnetic properties of AFM  $\text{Co}_3\text{O}_4$  nanoparticles has become significant because it is

involved in many advanced chemical and physical applications such as catalysis, sensors, magnetic materials, and energy storage [12,15,17]. In particular, many researchers have focused on the weak ferromagnetism below the Néel temperature and exchange anisotropy of the AFM  $\text{Co}_3\text{O}_4$  nanoparticles [12–14,18–20]. The bulk  $\text{Co}_3\text{O}_4$  compound is antiferromagnetic with a Néel temperature about 40 K, and has a normal cubic spinel structure with a lattice constant of 0.808 nm [21]. The  $\text{Co}_3\text{O}_4$  unit cell contains 16  $\text{Co}^{3+}$  octahedral ions exhibiting diamagnetism and eight  $\text{Co}^{2+}$  tetrahedral ions ordered antiferromagnetically [21]. However, the Néel temperature of the  $\text{Co}_3\text{O}_4$  nanoparticle is size dependent. In addition, the hysteresis loop and loop shift of the  $\text{Co}_3\text{O}_4$  nanoparticle have been observed at low temperature [13,18,19]. In this paper, we present the magnetic properties of AFM  $\text{Co}_3\text{O}_4$  nanoparticles with an average diameter around 30 nm.

## 2. Experimental details

The AFM  $\text{Co}_3\text{O}_4$  nanoparticles were synthesized by a solution-based method. All the reagents used in our experiments were analytically pure and were purchased from Beijing Chemical Reagent Company. A mixture of 2.5 mmol  $\text{CoCl}_2 \cdot 6\text{H}_2\text{O}$  and 10 mmol  $(\text{NH}_2)_2\text{CO}$  was dissolved into the deionized water to form the precursor solution. Then the precursor solution was transferred into a Teflon-lined stainless steel autoclave of 65 ml capacity. The autoclave was sealed and then heated for 10 h at

\* Corresponding author. Tel.: +86 10 82648119; fax: +86 10 82649531.

E-mail address: [jluo@aphy.iphy.ac.cn](mailto:jluo@aphy.iphy.ac.cn) (J. Luo).

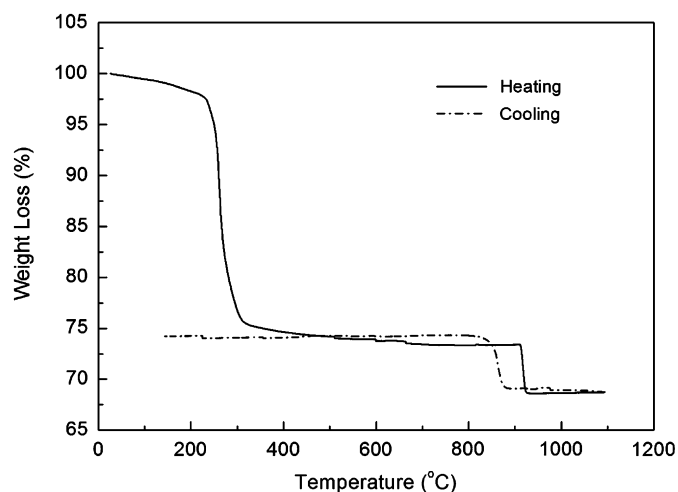
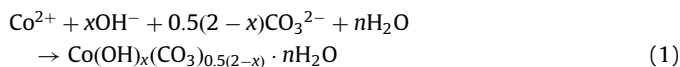


Fig. 1. TGA curves of the as-prepared precipitates.

100 °C. The precipitates were collected by centrifuging and washed several times by deionized water to remove any impurities after the autoclave cooled to room temperature naturally. The washed precipitates were then dried at 60 °C for 12 h. According to the wide-angle powder X-ray diffraction (XRD) pattern, the intermediate product was cobalt hydroxide carbonate with the chemical formula  $\text{Co}(\text{OH})_x(\text{CO}_3)_{0.5(2-x)} \cdot n\text{H}_2\text{O}$ , and the corresponding chemical reaction in the autoclave could be expressed as [22]



The calcination temperature was set according to our TGA measurement in dry air by TA-Q600. Fig. 1 shows that the decomposition temperature of the product is around 320 °C. Thereby, the product was calcinated at 380 °C for 4 h. Another decomposition reaction at 920 °C associated with the decomposition of  $\text{Co}_3\text{O}_4$  into  $\text{CoO}$  and  $\text{O}_2$  is also presented on the TGA curve, which can be confirmed by the weight loss percentage. As shown in Fig. 1, this reaction is reversible since the weight loss is compensated when the sample is cooled down to 880 °C.

Phase identification and structure analysis of the sample have been carried out by XRD using a Rigaku D/max 2500 diffractometer with  $\text{Cu-K}\alpha$  radiation (50 kV  $\times$  250 mA) and a graphitic monochromator. XRD data were collected by a step-scan mode with a step width of  $2\theta = 0.02^\circ$  and a sampling time of 1 s. A field emission scanning electron microscope (FESEM, FEI-Sirion) was used to characterize the morphology of the AFM  $\text{Co}_3\text{O}_4$  nanoparticles. The magnetic properties of  $\text{Co}_3\text{O}_4$  nanoparticles were measured using a superconducting quantum interference device (SQUID) magnetometer.

### 3. Results and discussion

Fig. 2 shows the XRD pattern of the resultant  $\text{Co}_3\text{O}_4$  product. All the peak can be exclusively indexed to the cubic spinel  $\text{Co}_3\text{O}_4$  structure (space group  $\text{Fd}\bar{3}\text{m}$ ), and no trace of other impurities is observed. The lattice constant calculated from the XRD pattern is 0.80843(2) nm. The grain size, which is in the range of 29–31 nm, has been estimated by the Scherrer formula. Particularly, the instrument influence has been eliminated by subtracting the peak width of the standard materials  $\text{LaB}_6$ . The size distribution of

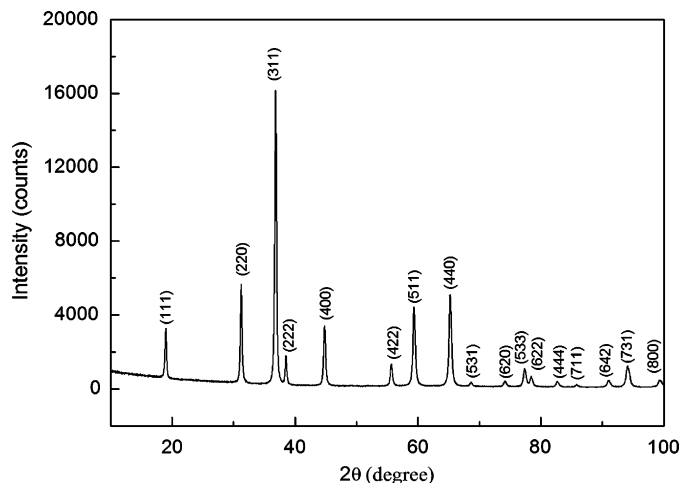


Fig. 2. XRD pattern of the  $\text{Co}_3\text{O}_4$  nanoparticles.

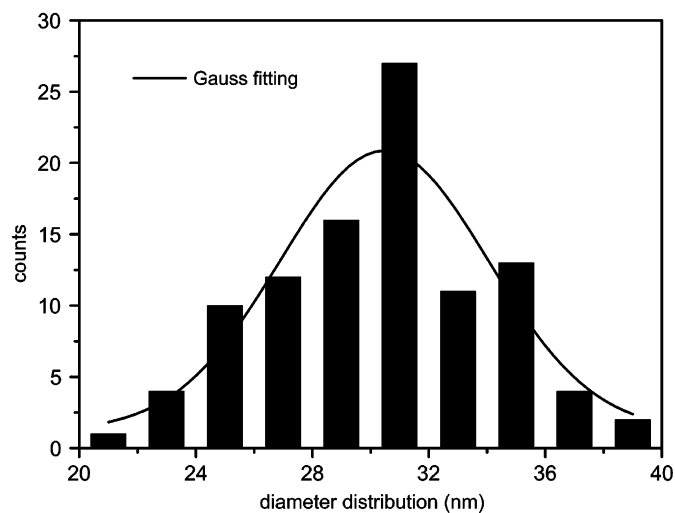


Fig. 3. Diameter distribution of the  $\text{Co}_3\text{O}_4$  nanoparticles.

$\text{Co}_3\text{O}_4$  nanoparticles has also been determined from the FESEM image (Fig. 3). The average diameter of the nanoparticles is around 30.6 nm (standard deviation 4.15), which agrees well with the calculated result based on the peak analysis of XRD pattern.

The morphology of AFM  $\text{Co}_3\text{O}_4$  has been investigated by FESEM. As shown in Fig. 4a, the sample consists of  $\text{Co}_3\text{O}_4$  nanorods with the diameter of a few hundred nanometers (averagely 400 nm) and lengths up to tens of microns. However, high-resolution FESEM images show these  $\text{Co}_3\text{O}_4$  nanorods are not single crystals but assembled by nanoparticles (see Fig. 4b, the sample in this SEM image is broken due to the ultrasonic treatment in ethanol). According to a previous report [22], the homogeneous precipitation method using urea generated cobalt compounds in the shape of nanorods or needles in a closed system. The authors of that report found that the as-prepared precipitates were indeed single-crystal nanorods and the diameter of the nanorod was controlled mainly by the synthesis temperature. However, after calcination the cobalt-hydroxide-carbonate nanorods were transformed into strings of  $\text{Co}_3\text{O}_4$  nanoparticles interconnected along the original longitudinal directions of the rods because the elimination of hydroxyl and carbonate groups and the formation of new phase during the

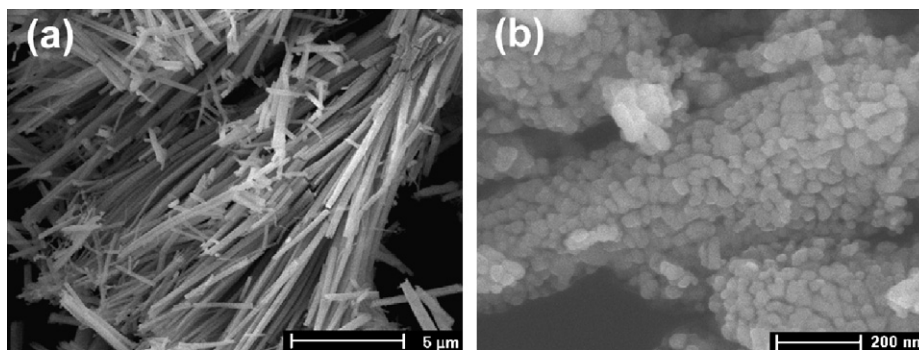


Fig. 4. (a) FESEM image of the  $\text{Co}_3\text{O}_4$  sample, (b) high-resolution FESEM image of the  $\text{Co}_3\text{O}_4$  nanorod.

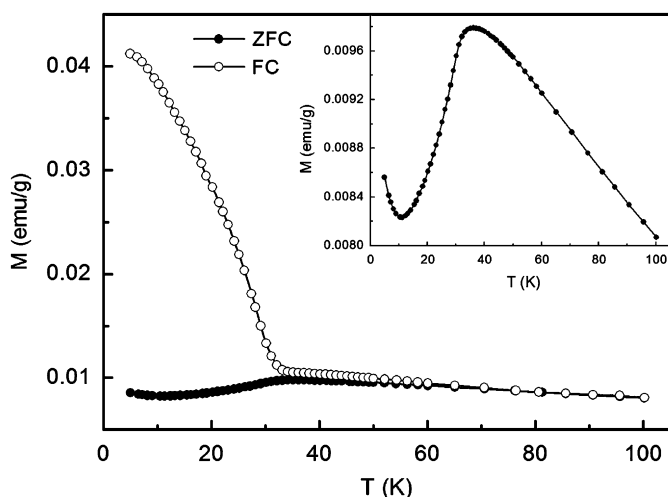


Fig. 5. Temperature dependence of the ZFC and FC magnetization curves in an applied field of 100 Oe. The inset is the ZFC curve exhibiting a broad peak around 37 K.

thermal decomposition caused the disruption of the original rod-like morphology and led to the one-dimensional beadlike assemblies. Our experimental result agrees well with the above growth mechanism proposed by Xu and Zeng [22].

The temperature dependence of the magnetization in a weak applied field of 100 Oe is shown in Fig. 5. In the field-cooled (FC) measurement, the sample is cooled from 100 K (above its Néel temperature) to 5 K in an external field of 50 kOe, and then the magnetization is recorded, on warming, in a field of 100 Oe. As for the zero-field-cooled (ZFC) measurement, the procedure is almost the same, except that there is no external field during cooling. A remarkable feature of the ZFC curve is the broad peak around 37 K (see the inset of Fig. 5), which corresponds to the Néel transition. A weak ferromagnetic (FM) behavior is indicated apparently by the strong bifurcation of the ZFC and FC curves at low temperature and the decreasing of the ZFC magnetization below 11 K. At 5 K, the FC magnetization is about five times of the ZFC magnetization; then the FC magnetization decreases dramatically with increasing temperature. Above the Néel temperature, the ZFC and FC curves become almost identical.

The Néel temperature of the AFM  $\text{Co}_3\text{O}_4$  nanoparticles is slightly lower than the bulk  $\text{Co}_3\text{O}_4$ , which has also been reported by other research groups [13,14,18,19,23]. This lower Néel temperature can be attributed to the finite size effect, which has succeeded in explaining the shift of the critical ordering

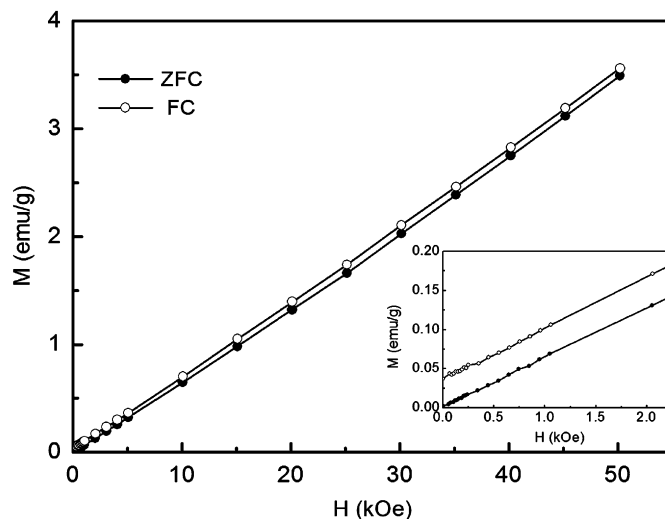


Fig. 6. Virgin magnetization curves at 5 K under ZFC and FC measurements. The inset shows the amplified curve at low field.

temperatures of ferromagnetic, ferrimagnetic and antiferromagnetic nanostructured materials [10,14,24]. According to the theory of finite-size scaling, the deviation of the transition temperature ( $T_N$ ) from that of the bulk should depend on the dimension ( $d$ ) of the nanostructured material as follows [10,23]:

$$[T_N(\infty) - T_N(d)]/T_N(\infty) = (d_0/d)^\lambda \quad (2)$$

In our case,  $T_N(\infty)$  and  $T_N(d)$  are the Néel temperatures of the bulk and nanostructured  $\text{Co}_3\text{O}_4$ , respectively.  $d_0$  is the extrapolated correlation length at 0 K, and  $\lambda$  is the shift exponent for the finite-size scaling. In our calculation, we choose the proposed value for the three-dimensional Heisenberg model ( $\lambda = 1.42$ ), which has been evaluated both theoretically and experimentally [10,25]. With the result of our experiment ( $T_N(d) = 37$  K for  $d = 30 \pm 1$  nm) and those of the latest reports ( $T_N(d) = 30$  K for  $d = 8$  nm and  $T_N(d) = 15 \pm 2$  K for  $d = 4.34$  nm) [13,14], the best fit values of  $T_N(\infty) = 38.6 \pm 0.5$  K and  $d_0 = 2.87 \pm 0.05$  nm are obtained. Considering the system error during measurement and different methods to determine the transition temperature,  $38.6 \pm 0.5$  K is a pretty reasonable value of  $T_N(\infty)$ . The value of  $d_0$  is roughly 3.5 times of the lattice constant of  $\text{Co}_3\text{O}_4$ , which fulfills its identification as a microscopic length scale. Therefore, we conclude that the shift of  $T_N$  can be well described by the effect of finite-size scaling.

The ZFC and FC virgin magnetization curves at 5 K are shown in Fig. 6, which are recorded after cooling the sample from 100 to 5 K in an applied magnetic field of 0 and 50 kOe, respectively. The magnetization is linearly dependent on the field and a shift toward large magnetization is observed for the FC virgin magnetization. The considerable magnetization indicates that the  $\text{Co}_3\text{O}_4$  nanoparticles are weak ferromagnetically ordered. For the bulk AFM materials, the net magnetization is zero due to the complete compensation of sublattice magnetizations. Hence, the origin of this weak ferromagnetism in our  $\text{Co}_3\text{O}_4$  nanoparticles can only be ascribed to the finite size effect. Different models have been proposed to explain the weak ferromagnetism in the antiferromagnetic nanostructured materials, such as CoO thin layers [10], NiO nanoparticles [11],  $\text{Co}_3\text{O}_4$  mesoporous [12],  $\text{Co}_3\text{O}_4$  nanoparticles [13,14,18,19,23,26], etc. Mainly, the weak ferromagnetism has been attributed to the uncompensated surface spins [10,11,16] or the partly inverted spinel structure probably by local electron hopping [19].

In order to gain further insight into the origin of the weak ferromagnetism in AFM  $\text{Co}_3\text{O}_4$  nanoparticles, the ZFC and FC hysteresis loops are measured with the same settings as those of virgin magnetization curves (shown in Fig. 7). As shown in the inset (b), the loop is open up to 40 kOe and the magnetization is almost linear with the field. For a system with an open loop up to a high field, it is believed that a high surface anisotropy and a spin-glass-like surface layer exist [11,13,26]. Fig. 8 shows the central portions of the ZFC and FC loops at 5 K. The ZFC hysteresis loop is symmetric about the origin with a coercivity ( $H_c$ ) of about 75 Oe, indicating a weak ferromagnetism. However, the FC loop is slightly broadened and shifted towards negative applied field, which exhibits the typical feature of an exchange bias system with an exchange bias field  $H_{\text{eb}} = (H_{\text{C1}}^{\text{FC}} + H_{\text{C2}}^{\text{FC}})/2$  around  $-390$  Oe. The exchange bias is an interfacial effect by the exchange coupling between AFM and FM layers, which induce an unidirectional anisotropy of the FM layer. Both the loop shift and exchange bias field are measures of the unidirectional exchange anisotropy. The observation of the loop shift, enhanced coercivity, as well as the exchange bias field indicate the existence of the AFM core and FM surface spin in our  $\text{Co}_3\text{O}_4$  nanoparticles, which can be attributed to the uncompensated surface spin due to the reduction of the coordination number at the surface of the AFM  $\text{Co}_3\text{O}_4$  nanoparticles.

As for the opening of the loop, a spin-glass-like surface system with multiple spin configurations is believed to be its origin [13].

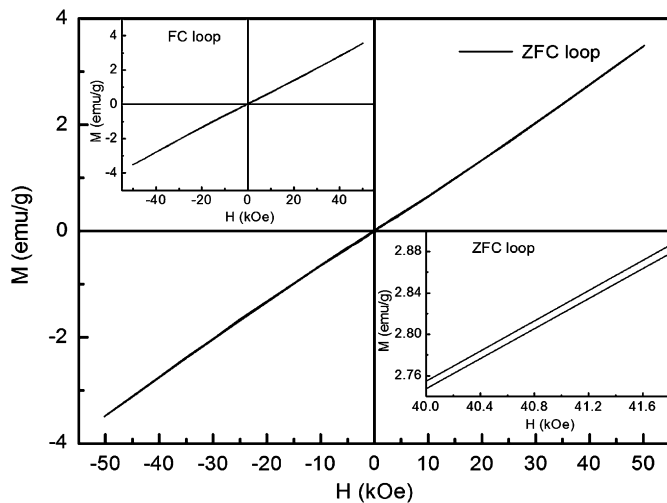


Fig. 7. ZFC hysteresis loop measured at 5 K. Insets are the FC hysteresis loop (a) and the high-field ZFC hysteresis loop opening up to 40 kOe (b).

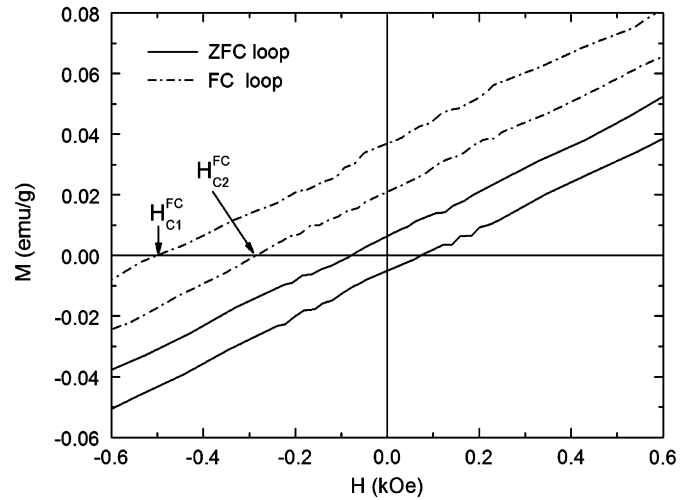


Fig. 8. Central portions of ZFC and FC hysteresis loop at low field showing an obvious loop shift.

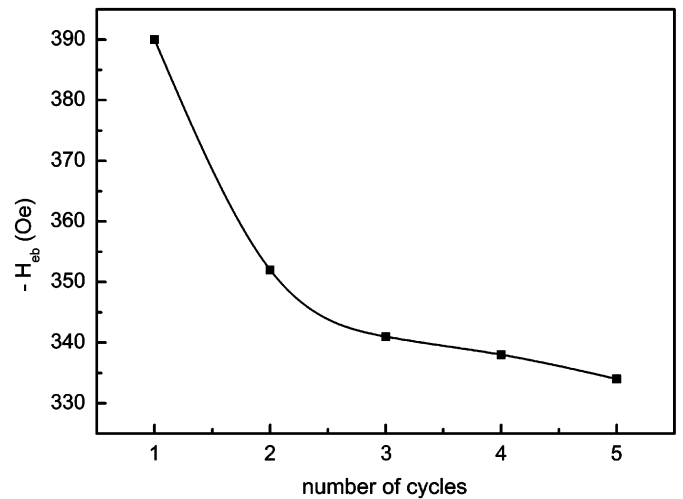


Fig. 9. Dependence of the exchange bias field on the number of cycles at 5 K.

According to Salaba et al. [13], the surface spins can be separated into two parts. One part is the frozen-in uncompensated spins, which do not reverse during the field cycling. The other part is the free spins, which can be aligned by an applied field. Thus, in one cycle of loop measurement, part of the magnetization (the frozen-in spins) is lost, leading to the opening of the loop. The existence of the spin-glass-like surface phase can be further confirmed by the training effect of the exchange bias field. To measure the training effect by a SQUID, the  $\text{Co}_3\text{O}_4$  nanoparticles were cooled from room temperature to 5 K in an applied field of 50 kOe, and then the hysteresis loop was recorded at 5 K. As shown in Fig. 9, the exchange bias field  $|H_{\text{eb}}|$  decreases with the number of cycles due to the loss of frozen-in spins.

The temperature dependence of the exchange field and coercivity is shown in Fig. 10. The hysteresis loop was recorded after the  $\text{Co}_3\text{O}_4$  nanoparticles were cooled from room temperature to the measure temperature in an external field of 50 kOe. Below the Néel temperature, both  $|H_{\text{eb}}|$  and  $H_c$  decrease with increasing temperature.  $|H_{\text{eb}}|$  and  $H_c$  approach the minimum around the Néel temperature due to the change of magnetic order from anti-ferromagnetic to paramagnetic.

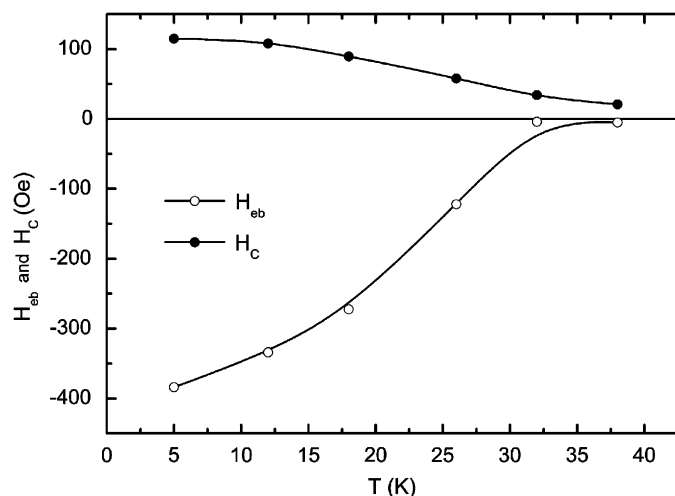


Fig. 10. Exchange bias field and coercivity as a function of temperature.

#### 4. Conclusion

In summary, the magnetic properties of AFM  $\text{Co}_3\text{O}_4$  nanoparticles prepared by hydrothermal method have been investigated. A deviation of its Néel temperature from the bulk has been found, which can be well described by the theory of finite-size scaling. At low temperature, the FC hysteresis loop exhibits enhanced coercivity and loop shift. An exchange bias system with the AFM core and FM surface spin is employed to explain anomalous magnetization of  $\text{Co}_3\text{O}_4$  nanoparticles. The finite size effect as well as the uncompensated surface spin is the origin of the weak ferromagnetism in the AFM  $\text{Co}_3\text{O}_4$  nanoparticles.

#### Acknowledgments

This work was supported by the Chinese Academy of Sciences and the Innovation Fund of Institute of Physics, Chinese Academy of Sciences.

#### References

- [1] S.H. Sun, C.B. Murray, D. Weller, L. Folks, A. Moster, *Science* 287 (2000) 1989.
- [2] P. Gambardella, S. Rusponi, M. Veronese, S.S. Dhesi, C. Grazioli, A. Dallmeyer, I. Cabria, R. Zeller, P.H. Dederichs, K. Kern, C. Carbone, H. Brune, *Science* 300 (2003) 1130.
- [3] V. Skumryev, S. Stoyanov, Y. Zhang, G. Hadjipanayis, D. Givord, J. Nogues, *Nature* 423 (2003) 850.
- [4] F. Dumestre, B. Chaudret, C. Amiens, P. Renaud, P. Fejes, *Science* 303 (2004) 821.
- [5] S. Mørup, C. Frandsen, *Phys. Rev. Lett.* 92 (2004) 217201.
- [6] J. Won, M. Kim, Y.W. Yi, Y.H. Kim, N. Jung, T.K. Kim, *Science* 309 (2005) 121.
- [7] M. Jamet, A. Barski, T. Devillers, V. Poydenot, R. Dujardin, P. Bayle-Guillemaud, J. Rothman, E. Bellet-Amalric, A. Marty, J. Cibert, R. Mattana, S. Tarentenko, *Nat. Mater.* 5 (2006) 653.
- [8] M.M. Ibrahim, S. Darwish, M. Seehra, *Phys. Rev. B* 51 (1995) 2955.
- [9] S. Gider, D. Awschalom, T. Douglas, S. Mann, M. Chaparla, *Science* 268 (1995) 77.
- [10] T. Ambrose, C.L. Chien, *Phys. Rev. Lett.* 76 (1996) 1743.
- [11] R.H. Kodama, S.A. Makhlof, A.E. Berkowitz, *Phys. Rev. Lett.* 79 (1997) 1393.
- [12] Y. Wang, C.M. Yang, W. Schmidt, B. Spliethoff, E. Bill, F. Schuth, *Adv. Mater.* 17 (2005) 53.
- [13] E.L. Salabas, A. Rumpelcker, F. Kleitz, F. Radu, F. Schüth, *Nano Lett.* 6 (2006) 2977.
- [14] D.A. Resnick, K. Gilmore, Y.U. Idzerda, M.T. Klem, M. Allen, T. Douglas, E. Arenholz, M. Young, *J. Appl. Phys.* 99 (2006) 08Q501.
- [15] I. Lopes, N.E. Hassan, H. Guerba, G. Wallez, A. Davidson, *Chem. Mater.* 18 (2006) 5826.
- [16] L. Néel, C. Dewitt, B. Dreyfus, P.D. de Gennes (Eds.), *Low Temp. Phys.*, Gordon and Beach, New York, 1962, p. 413.
- [17] P. Poizot, S. Laruelle, S. Grugeon, L. Dupont, J.M. Tarascon, *Nature* 407 (2000) 496.
- [18] S.A. Makhlof, *J. Magn. Magn. Mater.* 246 (2002) 184.
- [19] C. Nethravathi, S. Sen, N. Ravishankar, M. Rajamathi, C. Pietzonka, Bernd Harbrecht, *J. Phys. Chem. B* 109 (2005) 11468.
- [20] M. Sato, S. Kohiki, Y. Hayakawa, Y. Sonda, T. Babasaki, H. Deguchi, M. Mitome, *J. Appl. Phys.* 88 (2000) 2771.
- [21] W.L. Roth, *J. Phys. Chem. Solids* 25 (1964) 1.
- [22] R. Xu, H.C. Zeng, *J. Phys. Chem. B* 107 (2003) 12643.
- [23] Y. Ichihayagi, S. Yamada, *Polyhedron* 24 (2005) 2813.
- [24] Z.X. Tang, C.M. Sorensen, K.J. Klabunde, G.C. Hadjipanayis, *Phys. Rev. Lett.* 67 (1991) 3602.
- [25] K. Chen, A.M. Ferrenberg, D.P. Landau, *Phys. Rev. B* 48 (1993) 3249.
- [26] S. Li, H. Bi, B. Cui, F. Zhang, Y. Du, Z. Jiang, C. Yang, Q. Yu, Y. Zhu, *J. Appl. Phys.* 95 (2004) 7420.